IEEE Access
Multidisciplinary ⋮ Rapid Review ⋮ Open Access Journal

Received September 28, 2020, accepted October 11, 2020, date of publication October 21, 2020, date of current version October 30, 2020.

Digital Object Identifier 10.1109/ACCESS.2020.3032698

Low-Loss Light Guiding at the Subwavelength Scale in a Nanowire-Loaded Hybrid Bloch-Surface-Polariton Waveguide

WEIJING KONG[1], YU SUN[2], RUI MENG[1], AND XIAOCHANG NI[1]
[1]School of Electronic Engineering, Tianjin University of Technology and Education, Tianjin 300222, China
[2]School of Cyber Science and Technology, Beihang University, Beijing 100191, China

Corresponding author: Weijing Kong (kongweijing@tute.edu.cn)

This work was supported in part by the National Natural Science Foundation of China (NSFC) under Grant 61505145/61705012, and in part by the Natural Science Foundation of Tianjin City under Grant 18JCQNJC71000.

ABSTRACT We report the realization of strongly confined low-loss optical waveguiding at telecommunication wavelength by exploiting the hybridization of photonic modes guided by coupled dielectric mode and Bloch surface polaritons on the interface between one-dimensional photonic crystal and dielectric nanowire. Owing to the combined effects induced by the coupling between two types of guided modes, tight field localization in conjunction with significantly lower propagation loss can be achieved simultaneously. The characteristics of the hybrid modes are comprehensively numerically investigated through tuning key structural parameters of the coupled dielectric nanowire and its distance to the photonic crystal surface. The hybrid mode could effectively balance the compromise between the mode confinement and propagation loss for a wide geometrical parameter range. It reveals the hybrid mode is capable of enabling larger propagation distance (centimeter level) with subwavelength mode confinement, leading to a high figure of merit nearly one order of magnitude larger as compared to the conventional hybrid waves in dielectric-metal-based surface plasmon waveguides over the range of dimensions considered. The outstanding properties of the proposed guiding scheme could open up possibilities for a variety of high-performance intriguing nanophotonic components.

INDEX TERMS Optical waveguides, photonics, surface waves.

I. INTRODUCTION

Featuring simultaneously extraordinary optoelectronic properties and strong compatibility with chemical synthetic methods, dielectric-nanowire waveguides that enable ultra-low-loss lightwave transportation have been regarded as one of the most fundamental building blocks for photonic integrated components and circuits [1]–[5]. However, despite their attractive performance in long-range light transmission, the poor field confinement capability of these structures greatly hinders the further downscaling of the optical mode size beyond the diffraction limit. A promising strategy to overcome this limitation is to integrate them with metallic structures. Surface plasmon polaritons (SPPs), which employ the surface electromagnetic waves in the metallic nanostructures, has remarkable capability to manipulate light at the subwavelength scale beyond the diffraction limit. The extraordinary feature could miniaturize the physical dimensions of photonic components and has been regarded as a promising candidate in ultracompact photonic devices [6]–[11]. By combining metal with high-index nanowire, hybrid plasmonic waveguides (HPWs) have attracted particular attention [12]–[20]. The strong hybridization between plasmonic and dielectric modes enables efficient light transportation at deep subwavelength scale in conjunction with reasonable propagation distance, which outperforms the pure dielectric nanowires and conventional SPP structures. Despite the fact that the hybridized structures could improve the guiding performance to a certain extent, the associated Ohmic loss induced by the SPP metallic structures still restricts their further implementations in some practical applications. A variety of modified HPW waveguiding configurations have been proposed and demonstrated to alleviate the compromise between mode confinement and propagation

The associate editor coordinating the review of this manuscript and approving it for publication was Conrad Rizal.

loss [21]–[25]. However, the additional fabrication complexity brought in design is a major challenge in practical implementations of many modified HPW structures. Therefore, exploiting guiding configurations that could further improve the balance between filed confinement and modal loss, and thus allowing high compatibility with practical implementations remains a topic of active research.

Another technology that rivals SPPs is Bloch surface polariton (BSP) based counterparts excited in the all-dielectric truncated periodic multilayer structures [26]–[28]. Similar with SPP, BSP exhibits remarkable electric field enhancement at the surface, offering a promising route in high-performance light guiding and transmission [29], [30]. In contrast to SPP, BSP exhibits some unique capabilities for the realization of photonic components. Owing to the elimination of metal in the periodic dielectric stack, BSP waveguide could facilitate ultra-low-loss light transportation and thereby the propagation distance of the guided modes can be dramatically extended. Besides, in contrast to its SPP counterparts, the BSP structures can be designed more flexible at a much wider operating wavelength by either p- or s- polarization through engineering key structural parameters of the coupled dielectrics. Furthermore, by adopting semiconductor material, BSP structures could provide high refractive index contrast and thereby support tight field confinement. The applications of BSP structures in waveguiding schemes [31]–[34], optical sensing and fluorescence enhancement have been investigated and reported in recent years [35]–[42]. However, like other dielectric-based waveguides, the further downscaling of light to the subwavelength scale is still restricted by the diffraction limit, due to the excitation of BSP mode based on the internal reflection and refraction between multilayer dielectric layers. This poses a great threat to their practical implementations in the realization of high-performance integrated photonic devices. By integrating metal films and periodic multilayer structures, several typical studies have been proposed and demonstrated based on the hybridization between BSP mode and SPP mode, which show the prospect in enabling effectively balance between the mode confinement and propagation loss [43]–[45]. Nevertheless, compared with their SPP counterparts, limited attention has been paid to the research of improving the guiding performance of BSP in photonic components and devices up to date.

Here in this paper we would like to look into a more general waveguide configuration by integrating dielectric nanowire waveguides with BSP structures. For the investigated hybrid BSP waveguide, a truncated one-dimensional (1D) photonic crystal (PC) structure is explored to ensure the excitation of BSP mode. Leveraging their outstanding ability for ultra-low propagation loss and aiming at achieving simultaneous subwavelength field confinement. Comprehensive investigations on the guiding performance of the hybrid mode are conducted by tuning the waveguide's structural key parameters including the coupled dielectric nanowire and its distance to the truncated 1D PC structure surface. Owing to the hybridization between dielectric mode and BSP mode, the optical mode size can be squeezed down to the subwavelength scale while maintaining their remarkable, ultra-low-loss feature. In addition, the FOM (figure of merit) is carried out to provide a deeper understanding of their applications. The proposed structure could enable highly efficient light transmission in constructing integrated photonic devices.

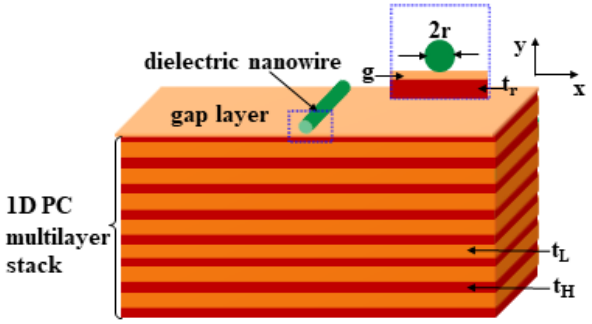

FIGURE 1. Schematic diagram of the investigated hybrid waveguide.

II. GEOMETRY AND OPTICAL PROPERTIES OF THE PROPOSED HYBRID WAVEGUIDE

Fig. 1 shows a schematic of the proposed hybrid BSP waveguide (HBSPW), where a high-index dielectric nanowire is separated from a truncated 1D PC dielectric multilayer stack with a homogeneously thick low-index dielectric filling the gap between the nanowire and multilayer stack. The high-index dielectric nanowire is buried in air cladding and the material of which is chosen as silicon (Si) with the radius denoted as r. The truncated 1D PC dielectric multilayer stack is configured to enable the excitation of BSP mode at the operating wavelength of $\lambda = 1550$ nm for an s-polarized input light using transfer matrix method [26]. It comprises of 7 alternating periods of high-index and low-index dielectric layers, with a terminated truncated high-index layer. In order to provide high compatibility with silicon photonic devices, the high-index and low-index dielectric layers are chosen as silicon (Si) and silica (SiO_2), respectively. Through engineering key structural parameters, the thicknesses of silicon and silica in each layer are set as $t_H = 234$ nm and $t_L = 320$ nm respectively, while the thickness of the terminated truncated layer is tuned to optimize the mode characteristics and denoted as t_r. The low-index gap layer is assumed to be as silica as well, and the size of the gap is represented by g. For the considered wavelength, the refractive indices of Si, SiO_2, and air are taken as $n_H = 3.476$, $n_L = 1.444$, and $n_c = 1$, respectively. In the following, the modal characteristics of the proposed waveguide are investigated in detail using the finite-element method (FEM) based on COMSOL^{TM}, and the guiding properties are analyzed by solving the eigenmode value with scattering boundary condition.

As a simple demonstration, we start our investigation by looking into the optical properties of the BSP mode sustained by the traditional truncated 1D PC structure. The thickness

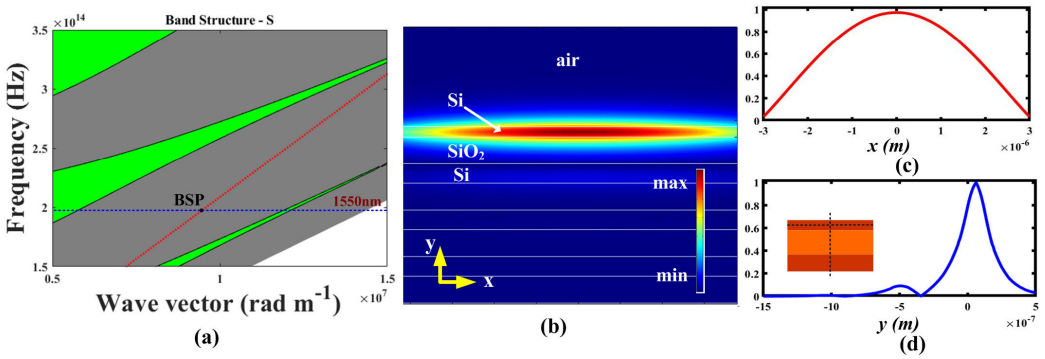

FIGURE 2. Band structure of the 1D PC structure for s-polarized input. The green region is the allowed band and the grey region is the band-gap. Dashed red line: light line for the excited mode effective index. Black solid circle: BSP mode. (b) Two-dimensional (2D) electric field distributions and the corresponding one-dimensional (1D) normalized field plots (c, d) of the BSP mode sustained by traditional truncated 1D PC structure with $t_r = 125$nm. Inset in (d): the field profiles are taken at the center of the truncated layer (horizontal dotted line) for (c) and (vertical dotted line) for (d) respectively.

of the truncated layer is chosen as $t_r = 125$ nm to guarantee the excitation of BSP mode. To demonstrate the excitation of BSP mode, the photonic band gap distribution of the 1D PC structure is calculated using transfer matrix method for s-polarized incidence [46]. As illustrated in Fig. 2(a), the allowed bands are indicated by the green regions and the forbidden bands are with the gray ones. The two dimensional (2D) electric field distribution of the excited BSP mode is investigated and depicted in Fig. 2(b), it shows that the electric filed is highly enhanced and confined in the truncated layer, indicating the excitation of the optical surface mode in the planned structure. Nevertheless, as shown in Fig. 2(c) and (d), for the 1D cross-sectional electric field distributions along the horizontal (x axis) and vertical (y axis) directions, the electric field is highly squeezed in the y direction while with a widespread distribution in the x direction, which would be not conducive to the application in integrated optoelectronic devices. For the considered working wavelength, the excitation position of the BSP mode is marked in the band structure by plotting the light line for the excited mode effective index in Fig. 2(a), we can observe that the BSP mode just locates inside the band gap of the band structure, ensuring the confinement of the mode on the surface.

Subsequently, the characteristics of the fundamental hybrid BSP mode sustained by the proposed HBSPW are briefly investigated first. Simulation results of the electric field distributions for the fundamental hybrid mode are depicted in Fig. 3. Similarly, both 2D modal profiles as well as the 1D cross-sectional electric field distributions are plotted to clearly demonstrate the field enhancement and confinement inside the truncated layer. As revealed in Fig. 3, with the geometric parameters of the proposed HBSPW are fixed at $t_r = 125$ nm, $r = 150$ nm, and $g = 20$ nm, owing to the hybridization of the dielectric mode and the BSP mode, the electric field is tightly squeezed and enhanced in the truncated layer and the gap region, showing a dramatic field confinement over the traditional BSP mode sustained by the 1D PC multilayer structure as shown above. In addition to the

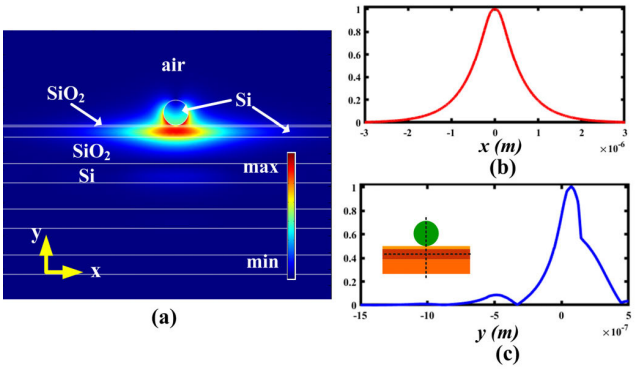

FIGURE 3. Two-dimensional (2D) electric field distributions (a) and the corresponding one-dimensional (1D) normalized field plots (b, c) of the hybrid BSP mode guided by the proposed HBSPW structure with $g = 20$nm, $t_r = 125$nm and $r = 150$nm. Inset in (c): the field profiles are taken at the center of the truncated layer (horizontal dotted line) for (b) and the dielectric nanowire (vertical dotted line) for (c) respectively.

prospect of enabling stronger optical confinement, the proposed HBSPW offers possibilities for achieving improved propagation distance over the traditional BSW, due to the gap introduced between the two coupled structures.

III. MODAL ANALYSIS OF THE PROPOSED HYBRID WAVEGUIDE

In order to obtain a comprehensive understanding of the optical performance of the proposed HBPSW structure, we conduct further investigations on the key geometric parameters' effects on the guided modes' properties. The hybridization between the dielectric mode and BSP mode can be optimized through tuning the gap size and other structural parameters of the waveguide, and thus enables efficient compromise between field confinement and propagation loss. Therefore, we first investigate the effect of the gap size on the properties of the guided hybrid BSP mode for waveguides with different truncated layer thicknesses. By fixing r at 150 nm and the truncated layer thickness t_r at 125 nm, increasing the gap size from 0 nm to 60 nm, the evolution of the field profiles

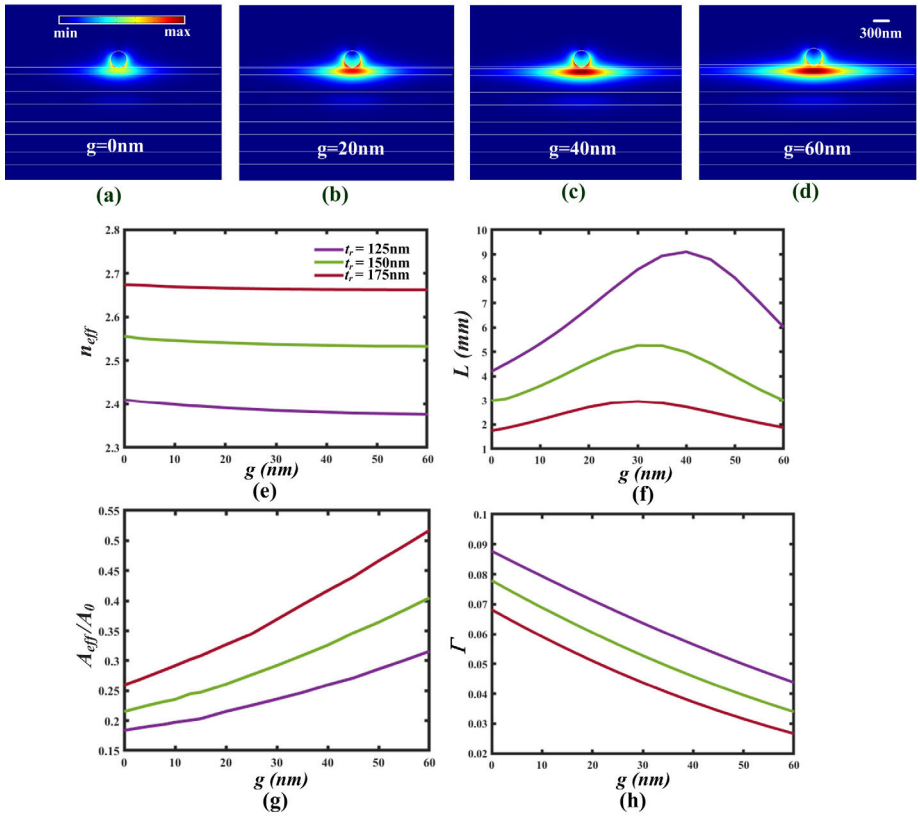

FIGURE 4. (a)-(d) Electric field distributions of the hybrid mode: (a) g=0nm; (b) g=20nm; (c) g=40nm; (d) g=60nm. Dependence of the modal properties on the gap size for different truncated layers: (e) modal effective index (n_{eff}); (f) propagation length (L); (g) normalized mode area (A_{eff}/A_0); (h) confinement factor in the considered gap region (Γ).

together with the field distributions of the hybrid mode for waveguides with the variation of gap size are depicted in Fig. 4(a)-(d). As clearly illustrated from the field profiles shown in the figures, by continuously increasing the gap size, the field profiles vary significantly as observable in the truncated layer and the gap region. When the gap size is small (g = 0 nm), the field is mainly confined at the gap region between the nanowire and the truncated layer, corresponding to the strongest coupling between the BSP and dielectric mode. As the gap size gets larger, the energy begins to shift towards the truncated layer. A further increase in the size of gap layer (e.g., g = 40 nm) results in the field enhancement shrinks in the gap region and the field localization decreases due to the weaker coupling between the BSP mode and dielectric mode. Finally, almost all of the energy could be stored inside the truncated layer when the gap size reaches a certain value (e.g., g = 60 nm), corresponding to the BSP-like mode. It is illustrated that with the varying of the gap size, the widened gap size results in the weakened field confinement from subwavelength field localization which will be quantitatively discussed in the following.

The hybrid modes' properties against the variation of the gap size are further investigated in order to gain deep understanding of the optical performance for the waveguide. The key modal parameters characterized the propagation mode include the mode effective index (n_{eff}), the propagation length (L), the normalized mode area (A_{eff}/A_0), and the confinement factor (Γ). Where, the mode effective index is the real part of the complex modal effective index N_{eff}. The propagation length featured the effective propagation loss of the mode is calculated using $L = \lambda/[4\pi Im(N_{eff})]$, whereas the effective mode area A_{eff} is calculated using the same method as in [12], [47], and A_0 is the diffraction-limited mode area defined as $\lambda^2/4$. The confinement factor is defined as the power ratio confined in the considered region to the total power of the waveguide.

As illustrated in Fig. 4(e)-(h), relatively dramatic modal behaviors can be observed within the whole parameter range, subwavelength mode size in conjunction with long propagation distance can be obtained concurrently. The continuously broadened gap size between the dielectric nanowire and multilayer dielectric stack has resulted in monotonic behavior in the modal effective index, the effective mode area and the power ratio inside the gap region, while leading to more complicated trends in the propagation length. From the results, it indicates that the optical performance of the hybrid mode is quite nice and tolerant to the deviations of the gap size. For waveguides with small gap size (e.g. g < 35 nm), the closely

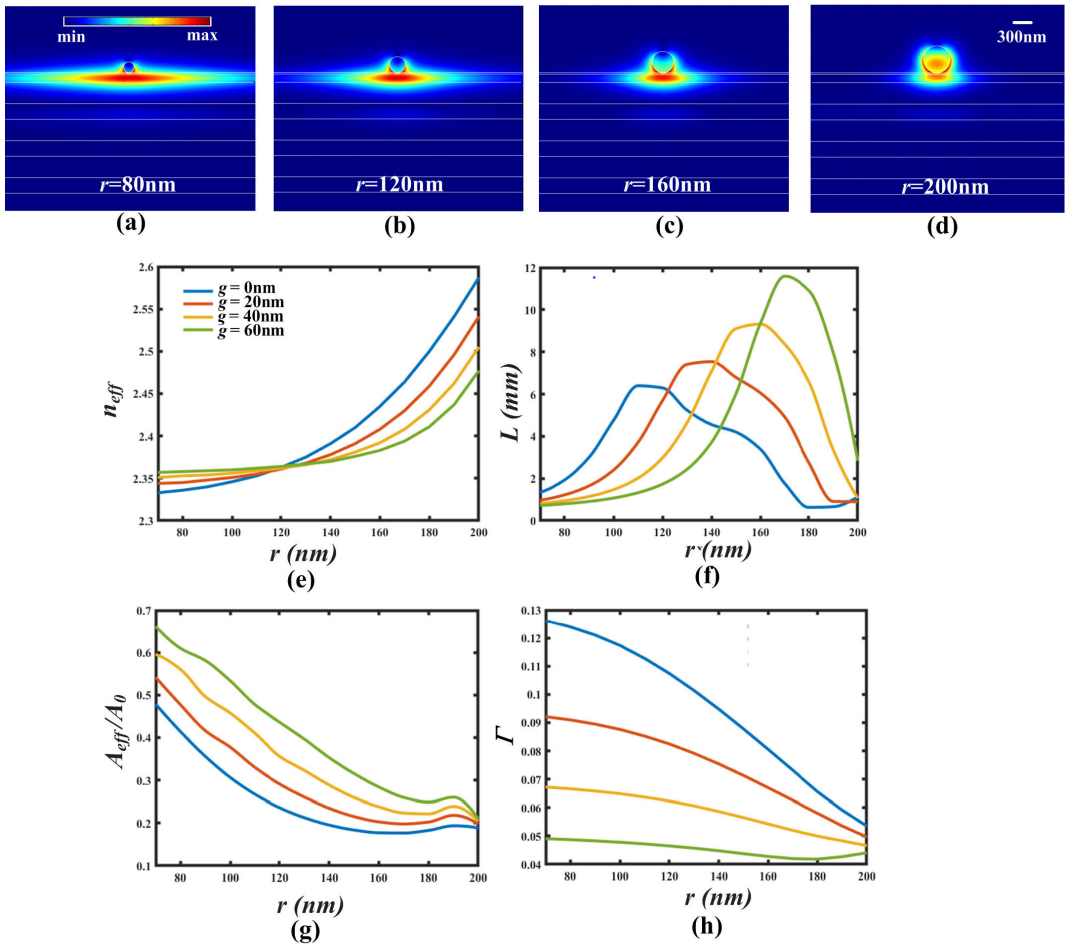

FIGURE 5. (a)-(d) Electric field distributions of the hybrid mode on the radius of the dielectric nanowire: (a) r=80nm; (b) r=120nm; (c) r=160nm; (d) r=200nm. (e)-(j) Dependence of the modal properties on the radius of the dielectric nanowire for different gap sizes: (e) modal effective index (n_{eff}); (f) propagation length (L); (g) normalized mode area (A_{eff}/A_0); (h) confinement factor in the considered gap region (Γ).

spaced multilayer dielectric stack and the dielectric nanowire strengthen the coupling between BSP and dielectric modes, leading to increased attenuation when the gap gets smaller. As the size of the gap gradually increases, the propagation distance enlarges along with a little sacrifice of the mode confined capability. As can be seen from Fig. 4(f), the propagation length of the hybrid mode can maintain at the millimeter level. Decreasing of the thickness of the truncated layer t_r could lead to further increased propagation distance, reaching centimeter level, while the corresponding mode area can be still held within the subwavelength scale. This marked feature of the proposed hybrid mode greatly facilitates the goal of achieving ultra-long propagation distance with subwavelength waveguiding. The translation occurs at moderate g (e.g. g = 35 nm), where the lowest propagation loss can be obtained. When the size of the gap is relatively large (e.g. g > 35 nm), the overall characteristics of the waveguide is mainly determined by the multilayer dielectric stack, resulting in increased propagation loss along with decreased field localization. The investigated mode properties combined with the corresponding field distributions indicate that the hybridized configuration could effectively confine the mode into subwavelength scale with ultra-low propagation loss.

To further reveal the guiding properties of the proposed hybrid waveguide, we then turn to explore the effect of the size of the dielectric nanowire on the guided mode's performance. In Fig. 5(a)–(d), the evolution of field profiles of the guided mode with the variation of dielectric nanowire are investigated. In order to simultaneously achieve both moderate propagation loss and small mode area, the thicknesses of the truncated layer and gap size are fixed at t_r = 125 nm and g = 20 nm respectively, while the size of the dielectric nanowire r varies within the range of 70 to 200 nm. As clearly demonstrated from the field profiles depicted in figures, an increase in the size of dielectric nanowire leads to the evolution of mode field from spreading inside the truncated layer toward concentrating inside the gap region and finally moving to the nanowire, corresponding to the

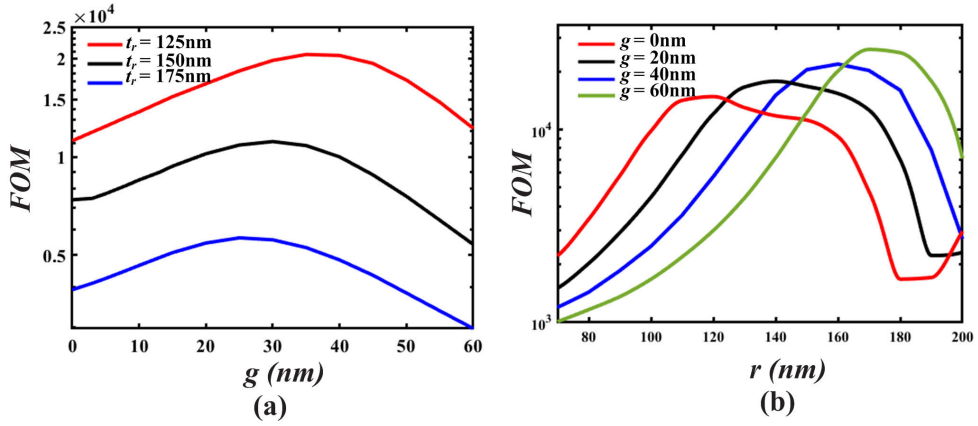

FIGURE 6. Dependence of the *FOM* on the gap size and the radius of the dielectric nanowire: (a) *FOM* for different gap sizes, based on the results in Figure 4; (b) *FOM* for different nanowire sizes, corresponding to the results in Figure 5.

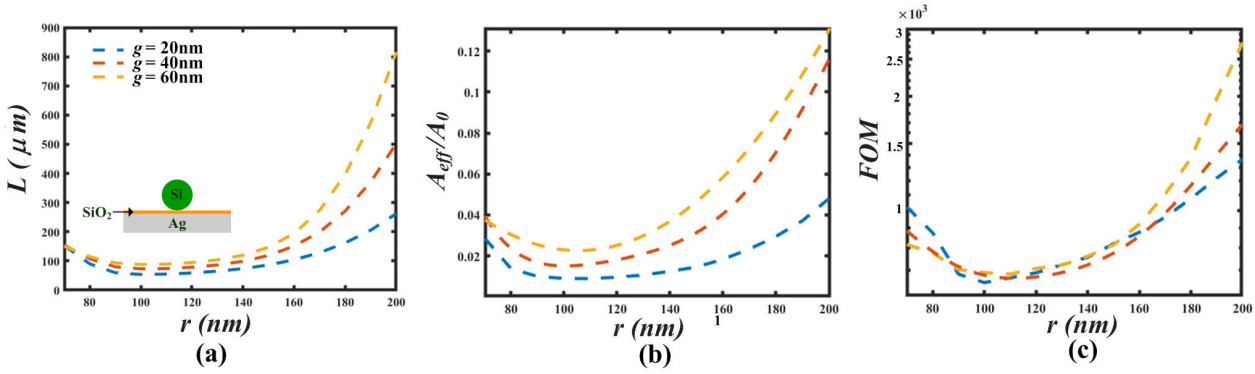

FIGURE 7. Dependence of the HPW modal properties on the radius of the dielectric nanowire: (a) propagation length (L); (b) normalized mode area (A_{eff}/A_0); (c) FOM; Inset in Fig. 7(a): geometry of the HPW.

hybrid mode behavior from BSP-like to dielectric-like. Indicated by the significant field enhancement and confinement inside the gap region, the hybridization between the BSP and dielectric modes is illustrated. Similar to the gap thickness studied above, the modal properties with the variation of the nanowire radius are further investigated to demonstrate the propagating capability. As can be noted, for the whole considered parameter region, the hybrid mode featured long propagation distance in conjunction with subwavelength mode confinement. In Fig. 5(e), as the nanowire gets bigger, the mode effective index n_{eff} increase monotonically. This trend seems more obvious for relatively large nanowire with a smaller gap size, due to the stronger interaction between the BSP and dielectric modes. Enlarging the dielectric nanowire leads to an extended propagation distance in combined with enhanced optical confinement with a decreasing mode area, owing to the increasing mode confinement in the low-index gap region. As revealed, the proposed structure effectively equilibrium the tradeoff between the propagation loss and mode confinement ability, which is superior to many of the existed hybrid waveguide schemes. As the nanowire gets to a moderate size, a shortened propagation distance with a decreased mode area can be observed, which can be attributed to the energy movement towards the nanowire. Simultaneously, for the decreasing gap size, reduced mode size and nonmonotonic propagation distance can be observed, which is consistent with the above discussions on the gap size. The corresponding confinement factor is also clearly denoted in Fig. 5(h), the mode confinement ability inside the gap region is calculated to indicate the transformation of optical power. It shows that the power ratio resided in the gap region slightly decreases. Our investigation also indicates the power ratio within the truncated layer declines gradually, while continuous enhancement in the confinement factor can be achieved inside the dielectric nanowire. The result is consistent with the field distributions shown in Fig. 5(a)-(d).

IV. FIGURE OF MERIT OF THE PROPOSED HYBRID WAVEGUIDE

To further benchmark the guiding properties of the hybrid BSP mode sustained by the proposed HBSPW structure. A figure of merit (FOM) dependent on the key geometric parameters is introduced to characterize the superiority. The FOM is defined as the ratio of the propagation length to the

effective mode size $2(A_{eff}/\pi)^{1/2}$. As shown in Fig. 6(a), when the gap layer varies from 0 to 60 nm, originating from the evolution of the coupled mode as investigated above, the non-monotonic behavior of FOM can be observable. Under the considered geometric parameter ranges, a thinner truncated layer at the multilayer dielectric surface could result in strong field confinement leading to enhanced FOM. From Fig. 6(b), we can observe that the FOM values from 10^3 to 10^4, and relatively high FOM can be obtained with the gradually increased gap and nanowire size, which can be attributed to the significantly increased propagation distance. As the gap size further increases, the FOM decreases along with the reduced propagation length and the sustainable enlarging mode area. On the other hand, originating from the combined effects of the thickened gap size and the increased nanowire, higher FOM values are accomplishable at a moderate nanowire size for a fixed gap size in the case of strong coupling hybrid mode. These results are consistent with the conclusions made in previous discussion.

To gauge the excellent optical performance of the proposed HBSPW, the properties of the fundamental plasmonic mode guided by the conventional HPW consisting of a dielectric nanowire supported by a metallic substrate with a low-index sandwiched gap in air cladding is also calculated. For fair comparison, the high-index dielectric nanowire is also selected as Si, and the radius of which are also set within the range 70-200nm, the gap size selected as SiO_2 is fixed at 20nm, 40nm, and 60nm respectively. Similar with the reported conventional HPW [12], the metallic substrate is chosen as Ag and the refractive index of which is $n_m = 0.1453 + 11.3587i$. As shown from the results in Fig. 7, we can see that under the considered parameter range, the propagation distance of the HPW travels from microns to a millimeter with a deep subwavelength mode confinement. It reveals that the effective mode area of the proposed HBSPW (see Fig. 5(g)) is slightly larger than that of the corresponding HPW. However, the propagation loss of the proposed HBSPW (see Fig. 5(f)) in these cases is significantly lower when compared to the conventional HPW. The drastically reduced propagation loss of HBSPW also leads to ultra-high FOM value, which is nearly one order of magnitude larger than that of HPW (see Fig. 6(b) and Fig. 7(c)). The results confirm the superior guiding properties of the proposed waveguiding scheme in offering long-range propagation distance with subwavelength mode confinement.

V. CONCLUSION

In conclusion, we have investigated the guiding properties of a hybrid BSP waveguide structure that consists of a dielectric nanowire placed on a 1D PC multilayer dielectric stack. The comprehensive understanding of the waveguide's performance could be enabled by tuning the key structural parameter including the size of the gap layer, dielectric nanowire and the thickness of the truncated layer. The investigations reveal that simultaneous realization of subwavelength light transportation and ultra-low propagation loss can be achieved under appropriate geometric parameters through the hybridization of BSP mode and dielectric mode. The proposed structure shows high compatibility with standard fabrication techniques and can be readily realized by employing atomic layer deposition (ALD) and chemical synthesis methods, exhibiting appealing potential capabilities in the realization in integrated photonic devices.

REFERENCES

[1] R. Yan, D. Gargas, and P. Yang, "Nanowire photonics," *Nature Photon.*, vol. 3, pp. 569–576, Oct. 2009.
[2] L. Tong, R. R. Gattass, J. B. Ashcom, S. He, J. Lou, M. Shen, I. Maxwell, and E. Mazur, "Subwavelength-diameter silica wires for low-loss optical wave guiding," *Nature*, vol. 426, no. 6968, pp. 816–819, Dec. 2003.
[3] C. J. Barrelet, A. B. Greytak, and C. M. Lieber, "Nanowire photonic circuit elements," *Nano Lett.*, vol. 4, no. 10, pp. 1981–1985, Oct. 2004.
[4] A. L. Pyayt, B. Wiley, Y. Xia, A. Chen, and L. Dalton, "Integration of photonic and silver nanowire plasmonic waveguides," *Nature Nanotechnol.*, vol. 3, no. 11, pp. 660–665, Nov. 2008.
[5] P. E. Landreman, H. Chalabi, J. Park, and M. L. Brongersma, "Fabry-Pérot description for Mie resonances of rectangular dielectric nanowire optical resonators," *Opt. Express*, vol. 24, no. 26, pp. 29760–29772, Dec. 2016.
[6] J. Gosciniak, V. S. Volkov, S. I. Bozhevolnyi, L. Markey, S. Massenot, and A. Dereux, "Fiber-coupled dielectric-loaded plasmonic waveguides," *Opt. Express*, vol. 18, no. 5, pp. 5314–5319, 2010.
[7] I. D. Rukhlenko, M. Premaratne, and G. P. Agrawal, "Guided plasmonic modes of anisotropic slot waveguides," *Nanotechnology*, vol. 23, no. 44, Oct. 2012, Art. no. 444006.
[8] J. Takahara, S. Yamagishi, H. Taki, A. Morimoto, and T. Kobayashi, "Guiding of a one-dimensional optical beam with nanometer diameter," *Opt. Lett.*, vol. 22, no. 7, pp. 475–477, Jul. 1997.
[9] S. A. Maier, P. G. Kik, H. A. Atwater, S. Meltzer, E. Harel, B. E. Koel, and A. A. G. Requicha, "Local detection of electromagnetic energy transport below the diffraction limit in metal nanoparticle plasmon waveguides," *Nature Mater.*, vol. 2, no. 4, pp. 229–232, Mar. 2003.
[10] P. Berini, "Long-range surface plasmon polaritons," *Adv. Opt. Photon.*, vol. 1, no. 3, pp. 484–588, Nov. 2009.
[11] Y. J. Guo, K. D. Xu, Y. Liu, and X. Tang, "Novel surface plasmon polariton waveguides with enhanced field confinement for microwave-frequency ultra-wideband bandpass filters," *IEEE Access*, vol. 6, pp. 10249–10256, Mar. 2018.
[12] R. F. Oulton, V. J. Sorger, D. A. Genov, D. F. P. Pile, and X. Zhang, "A hybrid plasmonic waveguide for subwavelength confinement and long-range propagation," *Nature Photon.*, vol. 2, no. 8, pp. 496–500, Aug. 2008.
[13] V. J. Sorger, Z. Ye, R. F. Oulton, Y. Wang, G. Bartal, X. Yin, and X. Zhang, "Experimental demonstration of low-loss optical waveguiding at deep sub-wavelength scales," *Nature Commun.*, vol. 2, no. 1, p. 331, May 2011.
[14] J. T. Kim, "CMOS-compatible hybrid plasmonic waveguide for subwavelength light confinement and on-chip integration," *IEEE Photon. Technol. Lett.*, vol. 23, no. 4, pp. 206–208, Feb. 15, 2011.
[15] C.-L. Zou, F.-W. Sun, C.-H. Dong, Y.-F. Xiao, X.-F. Ren, L. Lv, X.-D. Chen, J.-M. Cui, Z.-F. Han, and G.-C. Guo, "Movable fiber-integrated hybrid plasmonic waveguide on metal film," *IEEE Photon. Technol. Lett.*, vol. 24, no. 6, pp. 434–436, Mar. 2012.
[16] Y. Bian, Z. Zheng, X. Zhao, Y. Su, L. Liu, J. Liu, J. Zhu, and T. Zhou, "Guiding of long-range hybrid plasmon polariton in a coupled nanowire array at deep-subwavelength scale," *IEEE Photon. Technol. Lett.*, vol. 24, no. 15, pp. 1279–1281, Aug. 1, 2012.
[17] M. Talafi Noghani and M. H. Vadjed Samiei, "Analysis and optimum design of hybrid plasmonic slab waveguides," *Plasmonics*, vol. 8, no. 2, pp. 1155–1168, Mar. 2013.
[18] X. Guo, M. Qiu, J. Bao, B. J. Wiley, Q. Yang, X. Zhang, Y. Ma, H. Yu, and L. Tong, "Direct coupling of plasmonic and photonic nanowires for hybrid nanophotonic components and circuits," *Nano Lett.*, vol. 9, no. 12, pp. 4515–4519, Dec. 2009.
[19] H.-S. Chu, E.-P. Li, P. Bai, and R. Hegde, "Optical performance of single-mode hybrid dielectric-loaded plasmonic waveguide-based components," *Appl. Phys. Lett.*, vol. 96, no. 22, May 2010, Art. no. 221103.
[20] J. Zhu, Z. Xu, W. Xu, D. Fu, and S. Song, "New surface plasmon polariton waveguide based on GaN nanowires," *Results Phys.*, vol. 7, pp. 381–384, Jan. 2017.

[21] M. Wu, Z. Han, and V. Van, "Conductor-gap-silicon plasmonic waveguides and passive components at subwavelength scale," *Opt. Express*, vol. 18, no. 11, pp. 11728–11736, May 2010.
[22] D. Dai and S. He, "A silicon-based hybrid plasmonic waveguide with a metal cap for a nano-scale light confinement," *Opt. Express*, vol. 17, no. 19, pp. 16646–16653, Sep. 2009.
[23] Y. Bian, Z. Zheng, Y. Liu, J. Liu, J. Zhu, and T. Zhou, "Hybrid wedge plasmon polariton waveguide with good fabrication-error-tolerance for ultra-deep-subwavelength mode confinement," *Opt. Express*, vol. 19, no. 23, pp. 22417–22422, Nov. 2011.
[24] J. Zhang, L. Cai, W. Bai, Y. Xu, and G. Song, "Hybrid plasmonic waveguide with gain medium for lossless propagation with nanoscale confinement," *Opt. Lett.*, vol. 36, no. 12, pp. 2312–2314, Jun. 2011.
[25] C.-C. Huang, "Hybrid plasmonic waveguide comprising a semiconductor nanowire and metal ridge for low-loss propagation and nanoscale confinement," *IEEE J. Sel. Topics Quantum Electron.*, vol. 18, no. 6, pp. 1661–1668, Nov. 2012.
[26] P. Yeh, A. Yariv, and A. Y. Cho, "Optical surface waves in periodic layered media," *Appl. Phys. Lett.*, vol. 32, no. 2, pp. 104–105, Jan. 1978.
[27] R. D. Meade, K. D. Brommer, A. M. Rappe, and J. D. Joannopoulos, "Electromagnetic bloch waves at the surface of a photonic crystal," *Phys. Rev. B, Condens. Matter*, vol. 44, no. 19, pp. 10961–10964, Nov. 1991.
[28] W. M. Robertson, "Experimental measurement of the effect of termination on surface electromagnetic waves in one-dimensional photonic bandgap arrays," *J. Lightw. Technol.*, vol. 17, no. 11, pp. 2013–2017, Nov. 1999.
[29] A. Sinibaldi, N. Danz, E. Descrovi, P. Munzert, U. Schulz, F. Sonntag, L. Dominici, and F. Michelotti, "Direct comparison of the performance of bloch surface wave and surface plasmon polariton sensors," *Sens. Actuators B, Chem.*, vol. 174, pp. 292–298, Nov. 2012.
[30] M. Shinn and W. M. Robertson, "Surface plasmon-like sensor based on surface electromagnetic waves in a photonic band-gap material," *Sens. Actuators B, Chem.*, vol. 105, no. 2, pp. 360–364, Mar. 2005.
[31] Y.-C. Hsu and L.-W. Chen, "Bloch surface wave excitation based on coupling from photonic crystal waveguide," *J. Opt.*, vol. 12, no. 9, Sep. 2010, Art. no. 095709.
[32] E. Descrovi, T. Sfez, M. Quaglio, D. Brunazzo, L. Dominici, F. Michelotti, H. P. Herzig, O. J. F. Martin, and F. Giorgis, "Guided bloch surface waves on ultrathin polymeric ridges," *Nano Lett.*, vol. 10, no. 6, pp. 2087–2091, Jun. 2010.
[33] T. Sfez, E. Descrovi, L. Yu, D. Brunazzo, M. Quaglio, L. Dominici, W. Nakagawa, F. Michelotti, F. Giorgis, O. Martin, and H. Herzig, "Bloch surface waves in ultrathin waveguides: Near-field investigation of mode polarization and propagation," *J. Opt. Soc. Amer. B, Opt. Phys.*, vol. 27, no. 8, pp. 1617–1625, Aug. 2010.
[34] D. Aurelio and M. Liscidini, "Electromagnetic field enhancement in bloch surface waves," *Phys. Rev. B*, vol. 96, no. 4, Jul. 2017, Art. no. 045308.
[35] V. N. Konopsky and E. V. Alieva, "A biosensor based on photonic crystal surface waves with an independent registration of the liquid refractive index," *Biosensors Bioelectron.*, vol. 25, no. 5, pp. 1212–1216, Jan. 2010.
[36] F. Giorgis, E. Descrovi, C. Summonte, L. Dominici, and F. Michelotti, "Experimental determination of the sensitivity of Bloch surface waves based sensors," *Opt. Express*, vol. 18, no. 8, pp. 8087–8093, Aug. 2010.
[37] V. Paeder, V. Musi, L. Hvozdara, S. Herminjard, and H. P. Herzig, "Detection of protein aggregation with a bloch surface wave based sensor," *Sens. Actuators B, Chem.*, vol. 157, no. 1, pp. 260–264, Sep. 2011.
[38] W. Kong, Z. Zheng, Y. Wan, S. Li, and J. Liu, "High-sensitivity sensing based on intensity-interrogated bloch surface wave sensors," *Sens. Actuators B, Chem.*, vol. 193, pp. 467–471, Mar. 2014.
[39] L. Fornasari, F. Floris, M. Patrini, G. Canazza, G. Guizzetti, D. Comoretto, and F. Marabelli, "Fluorescence excitation enhancement by Bloch surface wave in all-polymer one-dimensional photonic structure," *Appl. Phys. Lett.*, vol. 105, no. 5, pp. 053303–053305, Aug. 2014.
[40] K. Toma, E. Descrovi, M. Toma, M. Ballarini, P. Mandracci, F. Giorgis, A. Mateescu, U. Jonas, W. Knoll, and J. Dostálek, "Bloch surface wave-enhanced fluorescence biosensor," *Biosensors Bioelectron.*, vol. 43, pp. 108–114, May 2013.
[41] L. Fornasari, F. Floris, M. Patrini, D. Comoretto, and F. Marabelli, "Demonstration of fluorescence enhancement via bloch surface waves in all-polymer multilayer structures," *Phys. Chem. Chem. Phys.*, vol. 18, no. 20, pp. 14086–14093, 2016.
[42] E. Gonzalez-Valencia, R. A. Herrera, and P. Torres, "Bloch surface wave resonance in photonic crystal fibers: Towards ultra-wide range refractive index sensors," *Opt. Express*, vol. 27, no. 6, pp. 8236–8245, Mar. 2019.
[43] Y. Wan, Z. Zheng, X. Shi, Y. Bian, and J. Liu, "Hybrid plasmon waveguide leveraging bloch surface polaritons for sub-wavelength confinement," *Sci. China Technol. Sci.*, vol. 56, no. 3, pp. 567–572, Jan. 2013.
[44] W. Kong, Y. Wan, W. Zhao, S. Li, and Z. Zheng, "Bloch-surface-polariton-based hybrid nanowire structure for subwavelength, low-loss waveguiding," *Appl. Sci.*, vol. 8, no. 3, p. 358, Mar. 2018.
[45] D. Zhang, Y. Xiang, J. Chen, J. Cheng, L. Zhu, R. Wang, G. Zou, P. Wang, H. Ming, M. Rosenfeld, R. Badugu, and J. R. Lakowicz, "Extending the propagation distance of a silver nanowire plasmonic waveguide with a dielectric multilayer substrate," *Nano Lett.*, vol. 18, no. 2, pp. 1152–1158, Feb. 2018.
[46] P. Yeh, A. Yariv, and C. S. Hong, "Electromagnetic propagation in periodic stratified media. I. General theory," *J. Opt. Soc. Amer.*, vol. 67, no. 4, pp. 423–438, Apr. 1977.
[47] Y. Bian and Q. Gong, "Long-range hybrid ridge and trench plasmonic waveguides," *Appl. Phys. Lett.*, vol. 104, no. 25, pp. 251115-1–251115-4, Jun. 2014.

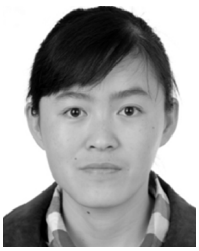

WEIJING KONG received the B.S. degree in telecommunication engineering from Liaocheng University, Liaocheng, Shandong, China, in 2006, the M.S. degree in precision instrument and machinery from Nanchang University, Nanchang, China, in 2009, and the Ph.D. degree in optical engineering from Beihang University, Beijing, China, in 2014. She was a Lecturer with the Tianjin University of Technology and Education, Tianjin, China. From 2018 to 2019, she was with Virginia Tech, as a Visiting Scholar. Her research interests include photonics and optical sensors, such as nanophotonics and biophotonics.

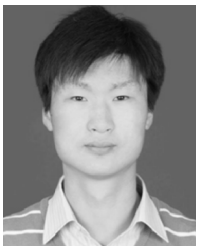

YU SUN received the B.S. and Ph.D. degrees in information and communication engineering from Beihang University, in 2008 and 2014, respectively. From 2014 to 2019, he was with Beijing Forestry University as a Lecturer for a period of three years and an Associate Professor. He has been with Beihang University as an Associate Professor since 2019. His research interests include photonics and machine learning, such as AI-based sensing signal identification.

RUI MENG received the B.S. degree in optoelectronic technology science and the Ph.D. degree in optical engineering from Tianjin University, Tianjin, China, in 2011 and 2019, respectively. He is currently with the School of Electronic Engineering, Tianjin University of Technology and Education, Tianjin. His research interest includes photoelectric detection technique.

XIAOCHANG NI received the B.S. degree in applied physics from Hebei University, Hebei, China, in 1998, and the M.S. and Ph.D. degrees from Tianjin University, Tianjin, China, in 2001 and 2004, respectively. Since March 2006, he has been with the Tianjin University of Technology and Education. He was with the Group of Application of Ultrafast Laser, School of Science, Università di Napoli Federico II, Napoli, Italy, as a Visiting Scholar, in 2008 and 2012, respectively. He is currently a Full Professor. His current research interests include ultrafast optics and nonlinear optical technologies, optical sensing, and photoelectric detection.